Available online at www.sciencedirect.com
ScienceDirect
Surface & Coatings Technology 202 (2008) 3257–3262
SURFACE & COATINGS TECHNOLOGY
www.elsevier.com/locate/surfcoat

Effects of incorporation of Si or Hf on the microstructure and mechanical properties of Ti–Al–N films prepared by arc ion plating (AIP)

Changjie Feng [a,b,*], Shenglong Zhu [b], Mingsheng Li [c], Li Xin [b], Fuhui Wang [b]

[a] School of Materials Science and Engineering, Nanchang Hangkong University, Nanchang, 330063, China
[b] State Key Laboratory for Corrosion and Protection, Institute of Metal Research, The Chinese Academy of Sciences, Wencui Road 62, Shenyang, 110016, China
[c] Jiangxi Key Laboratory of Surface Engineering, Jiangxi Science and Technology Normal University, Nanchang, 330013, China

Received 7 November 2006; accepted in revised form 29 November 2007
Available online 21 February 2008

Abstract

Ti–Al–N, Ti–Al–Si–N and Ti–Al–Hf–N films were deposited on 1Cr11Ni2W2MoV stainless steel by arc ion plating (AIP) with a $Ti_{70}Al_{30}$, a $Ti_{60}Al_{30}Si_{10}$ and a $Ti_{68}Al_{30}Hf_2$ cathode, respectively. The effects of Si or Hf addition on the composition, microstructure and mechanical properties of the Ti–Al–N films were investigated by EPMA, TEM, SEM, XRD, micro-hardness and wear tests. The results show that all the deposited films possessed B1 structure. With the incorporation of Si or Hf, the texture of Ti–Al–N films remarkably changed from preferred orientation of (220) to mixture broadened orientations of (111), (200) and (220), the mean crystallite size of Ti–Al–N decreased from ~90 nm to ~30 and ~15 nm and no peaks of crystalline Si_3N_4 were detected from XRD analyses. Due to the addition of Si or Hf, the micro-hardness of Ti–Al–N films increased remarkably from 23.5 Gpa to 33.6 or 29.5 GPa, and the wear resistance was also enhanced. The effects of incorporation of Si or Hf on the microstructure and mechanical properties of Ti–Al–N films are discussed.
© 2007 Elsevier B.V. All rights reserved.

Keywords: Ti–Al–Si–N; Ti–Al–Hf–N; Arc ion plating; Microstructure; Mechanical properties

1. Introduction

Transition metal nitrides, such as TiN, often combine the extreme hardness of covalent solids, the high melting temperature of ionic crystals, and the excellent electrical conductivity of transition metals [1–3]. The unique property of TiN makes it an excellent candidate for various applications in materials science, especially in the field of hard films. In order to further improve the performance of simple binary nitride TiN films, the addition of other light elements, such as Al [4–10] and Si [11–20], enlightened a new pathway for the designation and development of hard films. Ti–Al–N films have been attracting lots of concerns because they showed superior stability even at much elevated temperatures of approximately 800 °C [6–7], and are usually applied to various tools for high-speed machining process, dies, etc.[8–10]. The improved mechanical and oxidation properties were derived from the microstructure characterized by solid solution of Al into TiN [4,5]. However, Ti–Si–N films also attract large concerns with respect to hardness because they exhibit superhardness above 40 GPa [11–20].The superhardness is known to come from nanocomposite characteristics of nc-TiN/a-Si_3N_4 [11,13,14,20]. Therefore, one could assume that if Ti–Al–N and Ti–Si–N were mixed together, the formed quaternary nitrides might simultaneously have the unique properties of both two ternary composite films. Until now, only a few papers of the Ti–Al–Si–N system have been reported [21–25]. Therefore, studies on the microstructure and mechanical properties of the quaternary Ti–Al–Si–N films are strongly required.

As for the hard film process, the arc ion plating(AIP) technique is known to be a powerful method for TiN-based hard films because of many merits such as high ionization rate, high deposition rate, etc. [26,27]. While the AIP technique was successfully adopted for Ti–Al–N [5,7], it could not been

* Corresponding author. School of Materials Science and Engineering, Nanchang Hangkong University, Nanchang, 330063, China.
E-mail address: chjfengniat@sina.com (C. Feng).

0257-8972/$ - see front matter © 2007 Elsevier B.V. All rights reserved.
doi:10.1016/j.surfcoat.2007.11.036

Table 1
Typical deposition conditions for Ti–Al–N, Ti–Al–Si–N, Ti–Al–Hf–N films prepared by AIP

Base pressure	2.5×10^{-3} Pa
Working pressure	2.0 Pa
Working gas ratio	N_2/Ar ≈ 6
Deposition bias voltage	−600 V
Substrate temperature	220 °C
Arc currents	60 A
Deposition time	60 min
Typical film thickness	6–7 μm
Rotational velocity of substrate	10 rpm
Substrate current density	0.05 A/cm^2
Substrates to target distance	200 mm

applied to the Ti–Si–N system due to the inadequacy of the Si source. Up to now, most of the quaternary Ti–Al–Si–N films are prepared by magnetron sputtering [21,24], hybrid arc-sputtering method [22,23], or PECVD [25].

According to the numerous studies of the nanocomposite Ti–Si–N films, the maximum hardness is gained at the Si contents arranged in 5–13 at.%[18–20]. It is known that the Al content has great effects on the adhesion strength between Ti–Al–N films and their substrates [28–30]. Therefore, to ensure good adhesion property and enhanced hardness, a Ti–Al–Si–N film was prepared by arc ion plating (AIP) using alloy targets containing10 at.% of Si and 30 at% of Al in this study. Generally, a small amount of active element (AE), such as Y [13,15,31,32] and Hf [33], has significant effects on the microstructure and mechanical properties of TiN-based nitrides. In the present study, a Ti–Al–Hf–N film with lower Hf content and a reference Ti–Al–N film were also prepared by AIP from a $Ti_{68}Al_{30}Hf_2$ and a $Ti_{70}Al_{30}$ cathode. The effects of Si or Hf addition on the composition, microstructure and mechanical properties of the Ti–Al–N films were investigated by EPMA, TEM, SEM, XRD, micro-hardness and wear tests.

2. Experimental procedure

Polished 1Cr11Ni2W2MoV stainless steel substrates (size: 15 × 10 × 2 mm) were cleaned in an ultrasonic bath with alcohol and acetone successively and then put on the substrate holder in the vacuum chamber of a DH-4 arc ion plating system. Prior to deposition, the system was pumped down to a base pressure of 2.5×10^{-3} Pa and substrates were sputter-cleaned by Ar ion bombardment under a bias voltage of −1000 V with Ar atmosphere of 0.2 Pa for 10 min in order to remove the possible contaminations and to ensure good adhesion of the deposited films. Substrates were heated by resistant heaters set inside the chamber, and then Ti–Al–N, Ti–Al–Si–N and Ti–Al–Hf–N films were deposited by AIP with a $Ti_{70}Al_{30}$, a $Ti_{60}Al_{30}Si_{10}$ and a $Ti_{68}Al_{30}Hf_2$ cathode, respectively. The total working pressure (N_2+Ar) and the N_2 partial pressure were maintained at 2.0 Pa and 1.8 Pa, respectively. The deposition arc current and temperature were fixed at 60 A and 220 °C. Typical deposition conditions for the above films by the AIP system are summarized in Table 1.

The compositions of the deposited films were analyzed by EPMA. The microstructure and morphologies of the films were observed through Philips XL-30 SEM and TEM-2010. The phase analysis of the film was conducted by XRD with Cu Kα radiation. The crystalline size was also estimated from the full width at half maximum (FWHM) of X-ray diffraction peaks using the Scherrer formula [34], neglecting peak broadening due to micro-stresses of the films.

The Vickers hardness was measured using a SHIMADZU m-type micro-hardness tester with a pyramid load of 0.25 N applied for 15 s. In order to minimize the micro-hardness error, all the samples were polished before micro-hardness tests. The wear test was carried out using a ring-on-disk Amsler friction and wear-testing machine. A fine ground, hardened 45 carbon steel ring, size 50 mm diameter × 10 mm thickness, was used as the counterpart. The load was 0.47 kg and the sliding speed was 0.52 m/s. The total sliding time was 15 min and all the tests were conducted without lubrication. The total abrasive area was measured by a JXD-2 optical microscopy.

3. Results and discussions

3.1. Compositions

The compositions of Ti–Al–N, Ti–Al–Si–N and Ti–Al–Hf–N films deposited by AIP with a $Ti_{70}Al_{30}$, a $Ti_{60}Al_{30}Si_{10}$ and a $Ti_{68}Al_{30}Hf_2$ cathode, respectively, were analyzed by EPMA and the results are presented in Table 2. It can be seen that the Ti content in all the films were remarkably higher than that in the corresponding cathode, and the light elemental content change of Al or Si in the films compared to in the targets was opposite to that of Ti.

Coll et al. [35] indicated the re-sputtering yield of Al was higher than that of Ti when bombarded by low energy (E_I<1 keV). Lugscheider et al. [36] pointed that Al had a lower degree of ionization than Ti when evaporated in the AIP process. Anders [37] reported that in a cathodic arc plasma deposition of Ti–Si–N films, Ti ion has higher kinetic energy (~59 eV) than that (~34 eV) of Si ion. The kinetic energy of Ti ion exceeds the minimum displacement energy of the material which is in the range of 10–40 eV. Thus, the energetic Ti ions arriving at the growing film can displace surface atoms. The re-sputtering phenomenon would be caused preferentially by Ti ions rather than Si ions, comparing the kinetic energies of those ions.

The difference of re-sputtering yield, degree of ionization and ionic kinetic energy could account for the metallic deviation of the film from the target material. In our previous report [38] and other studies [19,39], the similar phenomenon was reported.

Table 2
The compositions of the Ti–Al–N, Ti–Al–Si–N and Ti–Al–Hf–N films analyzed by EPMA (M: the total elemental content in the film except N) at.%

Coatings	Ti/M	Al/M	Si/M	Hf/M	N
Ti–Al–N	81.82	18.28			53.07
Ti–Al–Si–N	68.65	25.109	6.05		55.09
Ti–Al–Hf–N	77.83	20.89		1.28	54.82

3.2. Microstructure

The surface and cross-sectional images of the Ti–Al–N, Ti–Al–Si–N and Ti–Al–Hf–N films are shown in Fig. 1. It can be seen that there were few small macroparticles on the surface of the Ti–Al–N film. However, due to the addition of Si or Hf, more and bigger macroparticles generated on the surfaces and incorporated in the films (see Fig. 1b,c).

In cathodic arc evaporation, three species create the film deposited on a substrate: ions of metal vapor, neutral metal vapor and the undesirable, but not inevitable, particles of various sizes and shapes commonly known as macroparticles.

The size and amount of macroparticles depend mainly on cathode material, current, and arc duration [40,41]. As far as the above films are concerned, they were deposited in the same conditions, but using different cathode target materials. The melting point of the target alloy mainly depends on its compositions and has great effects on the size and quantity of the macroparticles. According to the phase diagrams [42], the melting point of $Ti_{70}Al_{30}$ is higher than that of $Ti_{60}Al_{30}Si_{10}$, which may account for the increase in the size and amount of the macroparticles occurred to the Ti–Al–Si–N. The active element Hf may have influences on the arc duration, which generates more macroparticles on the Ti–Al–Hf–N films. The similar phenomenon was also observed in our previous study of Ti–Al–Y–N coatings deposited under the same conditions [32].

The plan-view TEM imagines of Ti–Al–N, Ti–Al–Si–N and Ti–Al–Hf–N films and their corresponding SAD patterns are presented in Fig. 2. The crystallites of the Ti–Al–N were remarkably refined by the addition Si or Hf, especially by Hf. It was found that smaller crystallites were located around bigger ones in the Ti–Al–Si–N films, and Ti–Al–Hf–N films showed more equiaxial refined grains. According to their corresponding SAD and typical XRD patterns (shown in Fig. 3), although the Si content was up to 6 at.% in the Ti–Al–Si–N films, any diffraction peaks for Si_3N_4 phase were not found in the samples. This result suggests that the silicon contributed to form an amorphous phase throughout the films [43–45]. The atomic radius of Hf is 2.16 Å, which is close to that of Ti (2.00 Å). Ti atoms are replaced by the Hf atoms to form solid solution as reported in references [33,46].The mean crystallite sizes were

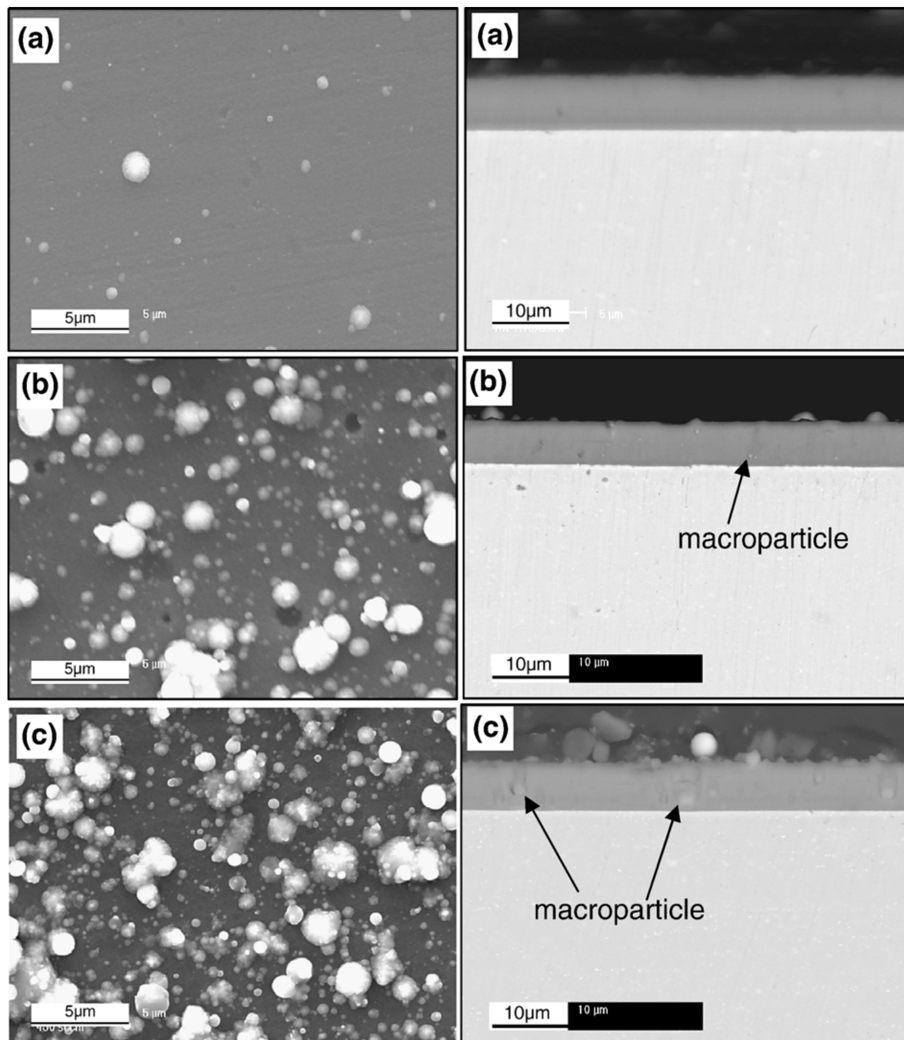

Fig. 1. Surface and cross-sectional images of (a) Ti–Al–N, (b) Ti–Al–Hf–N and (c) Ti–Al–Si–N films.

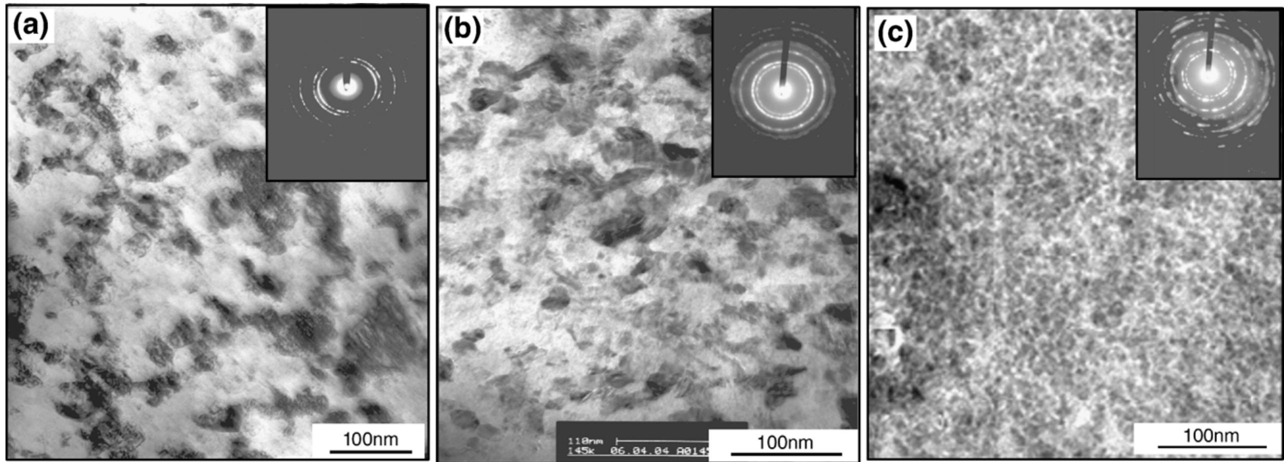

Fig. 2. Plan-view TEM imagines of (a) Ti–Al–N, (b) Ti–Al–Si–N and (c) Ti–Al–Hf–N films prepared by AIP and their corresponding SAD patterns.

about 90, 30 and 15 nm for Ti–Al–N, Ti–Al–Si–N and Ti–Al–Hf–N films estimated using the Scherrer formula [34].

Due to the addition of about 6 at.% of Si, the mean grain size of Ti–Al–N films decreased from ~90 to ~30 nm. However, compared to the grain size of $Ti_{0.67}Al_{0.23}Si_{0.09}N$ (~8 nm) [22] prepared by a hybrid cathodic arc-magnetron sputtering and Ti–Si–N (Si content: 0–21 at.%, grain size: 4.2–15 nm) [47] films prepared by magnetron sputtering process, the grain size of Ti–Al–Si–N films prepared herein by AIP was much bigger as shown in Fig. 2b. This can be explained by the following reasons: All the films in this article were deposited by AIP under relative high bias voltage of −600 V. It is well known that the increased bias voltage leads to the enhancement of the adatom surface mobility as well as the atomic diffusion [48], thereby enhancing grains growth, which contributes to the increase of grain size. On the other hand, the presence of the amorphous Si_3N_4 can suppress the grain growth of Ti–Al–N nanocrystals, leading to a finely grained dense microstructure. The Si content has significant influence on the grain size, and this is known as the percolation threshold [49,50]. The relative larger grain size of the Ti–Al–Si–N films may be due to the lower content of Si in the films and the deposition method of AIP.

Addition of Hf led to extensive grain refinement and a more equiaxed structure of the Ti–Al–N films. Kutschej et al. [33] also investigated the microstructure of $Ti_{1-x}Al_xN$ films alloyed with 2 at.%, 5 at.% and 10 at.% of Hf, respectively, and found that all the films showed fine grains with a domain size of 5–15 nm. The refined microstructure may be ascribed to the continuous nucleation process during the deposition induced by the active element [31,32].

3.3. X-ray

Fig. 3 shows the typical XRD patterns of the Ti–Al–N, Ti–Al–Hf–N and Ti–Al–Si–N films. All the films prepared herein had the same f.c.c. TiN structure. But the preferred orientation changed remarkably. As we discussed above, the Ti–Al–Si–N films consist of TiAlN nanocrystals embedded in a thin amorphous Si_3N_4 matrix and the Hf is incorporated in Ti–Al–N solid solution.

The Ti–Al–N film shows a remarkable (220) preferred orientation as we previously reported [38], and its sharp (220) reflection reveals that the film has a relatively coarse grain size. Due to the incorporation of Si or Hf, the alloyed Ti–Al–N films show mixture and prominent broadened textures of (220), (200) and (111). The XRD patterns are consistent with the micro-structure shown in Fig. 2.

The difference in the misorientation of the grains can be attributed to the addition of Si or Hf and the respective crystalline structure. This phenomenon, as suggested by Pelleg et al. [51], should be explained by energy considerations. The preferred orientation of films may be dependent upon the competition between the surface free energy and the strain energy. As the number of atoms in a grain is reduced, the excess surface free energy constitutes an increasingly important fraction of the total free energy. A small particle can reduce this excess free energy by changing its preferential orientation to one that has a lesser surface free energy. On the other hand,

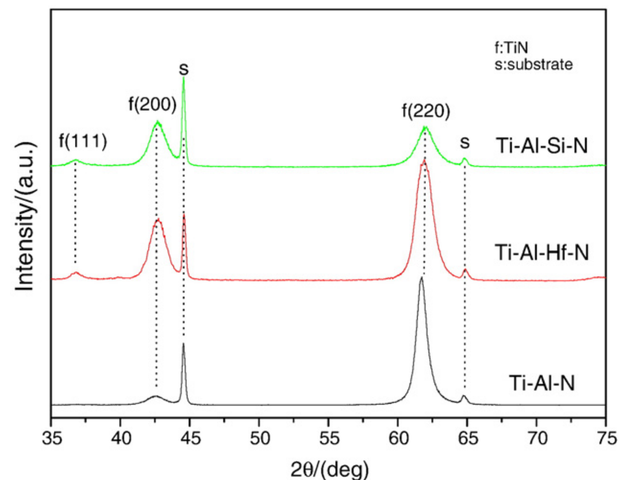

Fig. 3. The typical XRD patterns of the Ti–Al–N, Ti–Al–Hf–N and Ti–Al–Si–N films.

Table 3
The micro-hardness and abrasive area of the Ti–Al–N, Ti–Al–Si–N and Ti–Al–Hf–N films

Films	$Hv_{0.025}$ (GPa)	Abrasive area (mm^2)
Ti–Al–N	23.5±1.5	8.94
Ti–Al–Si–N	33.6±3.5	6.15
Ti–Al–Hf–N	29.5±2.7	7.58

due to the incorporation of Si or Hf in the Ti–Al–N films, the existence of amorphous Si_3N_4, or the greatly refined grains have great influences on the strain energy [11,27]. Peak broadening is generally attributed to reduction in the coherent diffracting domain size (related to grain size) and/or microstrains due to defects [48]. Similar peak broadening of the XRD patterns have been reported for ternary Ti–Si–N and quaternary Ti–Al–Si–N films [14,20,22,24]. This phenomenon was mainly attributed to the diminution of crystallite size.

3.4. Mechanical properties

The micro-hardness and abrasive area of the Ti–Al–N, Ti–Al–Si–N and Ti–Al–Hf–N films are summarized in Table 3. It reveals that, due to the incorporation of about 6 at.% Si and 1 at.% Hf into the Ti–Al–N(Al:18.28 at.%) films, the mean micro-hardness of the Ti–Al–N films increased significantly from 23.5 GPa to 33.6 and 29.5 GPa respectively.

The reasons [43] for the hardness increase of Ti–Al–N films with Si or Hf addition would be the grain boundary hardening both by strong cohesive energy in interphase boundaries[43,52] and by Hall–Petch relation derived from crystal size refinement [53], which were simultaneously caused by the percolation of amorphous Si_3N_4 into Ti–Al–N film. Other possible reason would be the solid-solution hardening of crystallites by Si dissolution into Ti–Al–N [54]. According to the compositions of the films in Table 2, all the films had the N content of more than 50 at.%. If all the films were stoichiometric nitrides as deduced from the XRD results in Fig. 3, the excess N atoms would be incorporated in the tetrahedral or octahedral gaps of the nitrides crystals, which could cause the distortion of the crystals and increase in hardness. In addition, almost random-orientated crystallites were considered related to the enhanced hardness.

However, the micro-hardness of the Ti–Al–Si–N films with mean grain size of 30 nm is larger than that of the Ti–Al–Hf–N films with equiaxial grains of 15 nm in size. This phenomenon seems to be a contravention to the Hall–Petch relationship [53]. According to the superhard mechanism of Ti–Si–N films proposed by Veprek [11], the amorphous Si_3N_4 play a vital role in the superhardness. The important influences of Si_3N_4 to the hardness of nanocomposite films are usually designated as percolation effect [49,50]. The possible reason for the above fact is that the contribution of amorphous Si_3N_4 to the increase of hardness exceeds that from the grain refinement induced by reactive element of Hf. Besides, the Hall–Petch relationship [55] is valid for crystallites larger than approximately 30 nm. For crystallites smaller than ~20 nm, the most important factor influencing the mechanical properties is the grain boundary sliding ability [56], which is made possible by a high density of defects at the grain boundaries.

It has been reported that the Si content has great effects on the hardness of the Ti–Si–N and Ti–Al–Si–N films [18,22,24,43]. Compared to the hardness of $Ti_{0.70}Al_{0.24}Si_{0.06}N$ films (42 GPa) prepared in a hybrid system of AIP and sputtering [22] and $Ti_{0.295}Al_{0.121}Si_{0.027}N_{0.557}$ films (38 GPa) prepared by sputtering [24], the micro-hardness of Ti–Al–Si–N films herein prepared by AIP was much lower. This can be explained by the following reasons. The crystallites of the Ti–Al–Si–N films are unequal as shown in Fig. 2b, and the mean grain size is relatively larger than those prepared by the other methods, which causes the reduction in hardness according to Hall–Petch relation [53]. Besides, during the nitride film preparation by AIP, macroparticles are generated and incorporated in the films, such as shown in Fig. 1. Because the macroparticles are relatively soft metal droplets from the targets, their incorporation into the films would result in the remarkable reduction of hardness [19]. Another possible reason would be the hardness measurement method. Due to the indentation size effect (ISE) [57,58], the hardness values obtained from nanoindentation test are always higher than those conducted in this article from the traditional micro-hardness tests.

The typical wear tracks of Ti–Al–N and Ti–Al–Si–N films are shown in Fig. 4. It is obvious that the wear resistance of Ti–Al–N films was much enhanced by the addition of Si. The protrusion of the substrate indicated the failure of the Ti–Al–N

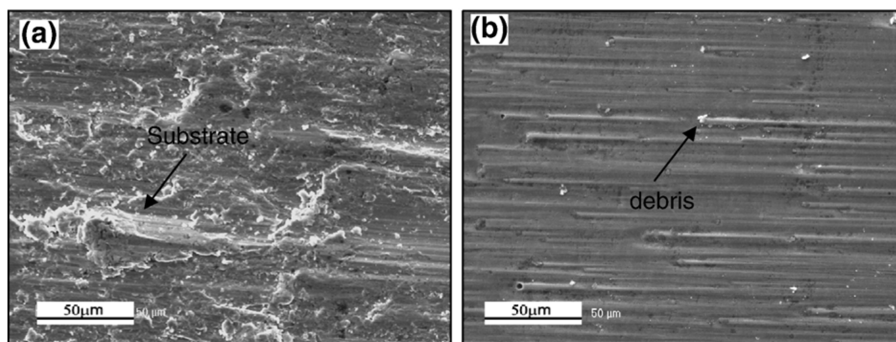

Fig. 4. The typical wear tracks of (a) Ti–Al–N and (b) Ti–Al–Si–N films.

film after the wear test. The debrises occurred on the track of Ti–Al–Si–N films were mainly composed of Fe, which were derived from the counterpart. The wear track of Ti–Al–Hf–N was very similar to that of the Ti–Al–Si–N film. According toTable 3, the abrasive areas of the deposited films are inversely proportional to their hardness values. The abrasive area of Ti–Al–Hf–N was smaller than that of Ti–Al–N film and close to that of the nanocomposite Ti–Al–Si–N film, which would be ascribed to the enhanced micro-hardness and improved wear resistance by Hf [33].

4. Conclusions

Ti–Al–N, Ti–Al–Si–N and Ti–Al–Hf–N films were deposited by arc ion plating with a $Ti_{70}Al_{30}$, a $Ti_{60}Al_{30}Si_{10}$ and a $Ti_{68}Al_{30}Hf_2$ cathode, respectively, and the effects of Si or Hf addition on the composition, microstructure and mechanical properties of the Ti–Al–N films were investigated. The obtained results are summarized as follows:

All the deposited films possessed B1crystalline structure. Due to the incorporation of Si or Hf, the texture of Ti–Al–N films remarkably changed from preferred orientation of (220) to mixture broadened orientations of (111), (200) and (220), and their mean crystalline sizes were significantly decreased from ~90 nm to ~30 and ~15 nm. No peaks of crystalline Si_3N_4 were detected from XRD analyses.

Due to the incorporation of Si or Hf, the mechanical properties of Ti–Al–N films were remarkably enhanced: the mean hardness of Ti–Al–N films was increased from 23.5 Gpa to 33.6 or 29.5 GPa, and the wear resistance was also improved. The macroparticles had large deleterious influences on the microstructure and mechanical properties of the deposited films. Much better mechanical properties of Ti–Al–Si–N and Ti–Al–Hf–N films could be obtained with lesser amount of macroparticles.

References

[1] A. Cselle, A. Barimani, Surf. Coat. Technol. 76–77 (1995) 712.
[2] J.-W. He, C.-D. Bai, K.-W. Xu, N.-S. Hu, Surf. Coat. Technol. 74–75 (1995) 387.
[3] P. Patsalas, C. Charitidis, S. Logothetidis, C.A. Dimitriadis, O. Valassiades, J. Appl. Phys. 86 (1999) 5296.
[4] W.D. Münz, J. Vac. Sci. Technol. A 4 (1986) 2717.
[5] O. Knotek, M. Bohmer, T. Leyendecker, J. Vac. Sci. Technol. A 4 (1986) 2695.
[6] D. McIntyre, J.E. Greene, G. Hakansson, J.-E. Sundgren, W.D. Münz, J. Appl. Phys. 67 (3) (1990) 1542.
[7] S. PalDey, S.C. Deevi, Mater. Sci. Eng. A 342 (2003) 58.
[8] M.C. Kang, I.-W. Park, K.H. Kim, Surf. Coat. Technol. 163–164 (2003) 734.
[9] S.G. Harris, E.D. Doyle, A.C. Vlasveld, P.J. Dolder, Surf. Coat. Technol. 146–147 (2001) 305.
[10] J.P. Urbanski, P. Koshy, R.C. Dewes, D.K. Aspinwall, Mater. Des. 21 (2000) 395.
[11] S. Veprek, Surf. Coat. Technol. 97 (1997) 15.
[12] S. Veprek, S. Reiprich, L. Shizi, Appl. Phys. Lett. 66 (20) (1995) 2640.
[13] Dayan Ma, Shengli Ma, Kewei Xu, Surf. Coat. Technol. 184 (2004) 182–187.
[14] Jun Bo Choi, Kurn Cho, Mi-Hye Lee, Kwang Ho Kim, Thin Solid Films 447–448 (2004) 365.
[15] X. Sun, J.S. Reid, E. Kolawa, M.-A. Nicolet, J. Appl. Phys. 81 (2) (1997) 656.
[16] M. Diserens, J. Patscheider, F. Levy, Surf. Coat. Technol. 120–121 (1999) 158.
[17] L. Le Brizoual, A. Granier, F. Clenet, P. Briaud, G. Lemperiere, G. Turban, Surf. Coat. Technol. 116–119 (1999) 922.
[18] Fanghua Mei, Nan Shao, Xiaoping Hu, et al., Mater. Lett. 59 (2005) 2442.
[19] Ryong Choi, In-Wook Park, Jong Hyun Park, Kwang Ho Kim, Surf. Coat. Technol. 179 (2004) 89–94.
[20] A. Bendavid, P.J. Martin, E.W. Preston, et al., Surf. Coat. Technol. 201 (2006) 4139.
[21] S. Carvalho, E. Ribeiro, L. Rebouta, F. Vaz, E. Alves, D. Schneider, Surf. Coat. Technol. 174–175 (2003) 984.
[22] In-Wook Park, Sung Ryong Choi, Ju Hyung Suh, Chan-Gyung Park, Kwang Ho Kima, Thin Solid Films 447–448 (2004) 443.
[23] I. Park, S.R. Choi, J.H. Suh, C. Park, K.H. Kim, Thin Solid Films 447–448 (2004) 443.
[24] Ning Jiang, Y.G. Shen, H.J. Zhang, S.N. Bao, X.Y. Houa, Mater. Sci.Eng. B 135 (2006) 1.
[25] Y.S. Li, S. Shimada, H. Kiyono, A. Hirose, Acta Mater. 54 (2006) 2041.
[26] P.C. Johnson, in: M.H. Francombe, J.L. Vossen (Eds.), Contemporary Preparative Techniques, Academic Press, London, 1989, p. 129.
[27] D.-Y. Wang, C.-L. Chsng, K.-W. Wong, et al., Surf.Coat. Technol. 120–121 (1999) 388.
[28] Kwang-Lung Lin, Wen-Hsiuan Chao, Cheng-Dau Wu, Surf. Coat. Technol. 89 (1997) 279.
[29] S.K. Wu, H.C. Lin, P.L. Liu, Surf. Coat. Technol. 124 (2000) 97.
[30] Changjie Feng, Mingsheng Li, Li Xin, et al., Oxid. Met. 65 (2006) 307.
[31] L.A. Donohue, D.B. Lewis, W.D. Münz, et al., Vacuum 55 (1999) 109.
[32] Mingsheng Li, Changjie Feng, Fuhui Wang, Weitao Wu, Mat. Sci. Forum 546–549 (2007) 1789.
[33] K. Kutschej, T.N. Fateh, P.H. Mayrhofer, M. Kathrein, P. Polcik, C. Mitterer, Surf. Coat. Technol. 200 (2005) 113.
[34] H.P. Klug, L.E. Alexander, X-ray Diffraction Procedures, Wiley, NewYork, 1974, p. 306.
[35] B.F. Coll, R. Fontana, A. Gates, P. Sathrum, Mater. Sci. Eng. A 140 (1991) 816.
[36] E. Lugscheider, O. Knotek, F. Loffler, et al., Surf. Coat. Technol. 76/77 (1995) 700.
[37] A. Anders, Appl. Phys. Lett. 80 (2002) 1100.
[38] Mingsheng Li, Fuhui Wang, Surf. Coat. Technol. 167 (2003) 197.
[39] Sung Ryong Choi, In-Wook Park, Sang Ho Kim, Kwang Ho Kim, Thin Solid Films 447–448 (2004) 371.
[40] I.I. Aksyonov, V.M. Khoroshikh, Review, Atominform, Moscow, 1984, p. 57.
[41] D.T. Tuma, C.I. Chen, D.K. Davies, J. Appl. Phy. 49 (7) (1978) 3821.
[42] http://www.crct.polymtl.ca/FACT/documentation.
[43] Jeong Suk Kima, Gyeng Joong Kima, et al., Surf. Coat. Technol. 193 (2005) 249.
[44] Yunshan Dong, Fanghua Mei, et al., Mater. Letter. 59 (2005) 171.
[45] Ping Zhang, Zhihai Cai, Wanquan Xiong, Surf. Coat. Technol. 201 (2007) 6819.
[46] E. Lugscheider, O. Knotek, H. Zimmermann, S. Hellman, Surf.Coat. Technol. 116–119 (1999) 239.
[47] Ye Xu, Liuhe Li, Xun Cai, Paul K. Chu, Surf. Coat. Technol. 201 (2007) 6824.
[48] R. Chandra, Davinder Kaur, Amit Kumar Chawla, et al., Mater. Sci. Eng. A 423 (2006) 111.
[49] S. Christiansen, M. Albrecht, H.P. Strunk, S. Veprek, J. Vac. Sci. Technol. B 16 (1) (1998) 19.
[50] S.H. Kim, J.K. Kim, K.H. Kim, Thin Solid Films 420–421 (2002) 360.
[51] J. Pelleg, L.Z. Zevin, S. Lungo, Thin Solid Films 197 (1991) 117–128.
[52] S. Veprek, J. Vac. Sci. Technol., A, Vac. Surf. Films 17 (1999) 2401.
[53] A. Lasalmonie, J.L. Strudel, J. Mater. Sci. 21 (1986) 1837.
[54] S. Carvalho, L. Rebouta, A. Cavaleiro, L.A. Rocha, J. Gomes, E. Alves, Thin Solid Films 398–399 (2001) 391.
[55] N.J. Petch, J. Iron Steel Inst. 174 (1953) 25.
[56] S. Zhang, D. Sun, Y. Fu, H. Du, Surf. Coat. Technol. 167 (2003) 113.
[57] N.A. Stelmashenko, M.G. Walls, L.M. Brown, Y.V. Milman, Acta. Metal1. 4l (1993) 2855.
[58] K.W. McElhaney, J.J. Vlassak, W.D. Nix, J. Mater. Res. 13 (1998) l300.